Published in final edited form as:
Eur J Radiol. 2006 August ; 59(2): 244–252.

Pulmonary Nodule Characterization: A Comparison of Conventional with Quantitative and Visual Semi-Quantitative Analyses Using Contrast Enhancement Maps Original Research

Iva Petkovska, MD, **Sumit K. Shah, PhD**, **Michael F. McNitt-Gray, PhD**, **Jonathan G. Goldin, MbChB PhD**, **Matthew S. Brown, PhD**, **Hyun J. Kim, MS**, **Kathleen Brown, MD**, and **Denise R. Aberle, MD**

Department of Radiological Sciences, David Geffen School of Medicine at University of California Los Angeles, Thoracic Imaging Research Group, 924 Westwood Blvd. Suite 650, Box 957319 Los Angeles, CA 90095-7319, USA

Abstract

Purpose— To determine whether conventional nodule densitometry or analysis based on contrast enhancement maps of indeterminate lung nodules imaged with contrast-enhanced CT can distinguish benign from malignant lung nodules.

Materials and Method— Thin section, contrast-enhanced CT (baseline, and post-contrast series acquired at 45, 90,180, and 360 seconds) was performed on 29 patients with indeterminate lung nodules (14 benign, 15 malignant). A thoracic radiologist identified the boundary of each nodule using semi-automated contouring to form a 3D region-of-interest (ROI) on each image series. The post-contrast series having the maximum mean enhancement was then volumetrically registered to the baseline series. The two series were subtracted volumetrically and the subtracted voxels were quantized into seven color-coded bins, forming a contrast enhancement map (CEM). Conventional nodule densitometry was performed to obtain the maximum difference in mean enhancement values for each nodule from a circular ROI. Three thoracic radiologists performed visual semi-quantitative analysis of each nodule, scoring each map for (a) magnitude and (b) heterogeneity of enhancement throughout the entire volume of the nodule on a 5-point scale. Receiver operator characteristic (ROC) analysis was conducted on these features to evaluate their diagnostic efficacy. Finally, 14 quantitative texture features were calculated for each map. A statistical analysis was performed to combine the 14 texture features to a single factor. ROC analysis of the derived aggregate factor was done as an indicator of malignancy. All features were analyzed for differences between benign and malignant nodules.

Results—Using 15 HU as a threshold, 93% (14/15) of malignant and 79% (11/14) of benign nodules demonstrated enhancement. The ROC curve when higher values of enhancement indicate malignancy was generated and area under the curve (AUC) was 0.76. The visually scored magnitude of enhancement was found to be less effective in distinguishing malignant from benign lesions, with an average AUC of 0.62. The visually scored pattern of enhancement was found to be more effective

Corresponding author: Iva Petkovska MD ipetkovska@mednet.ucla.edu, Phone: (310) 794-8982, Fax: (310) 794-8647.

Email addresses: Iva Petkovska MD ipetkovska@mednet.ucla.edu, Sumit K. Shah PhD sshah@mednet.ucla.edu, Michael F. McNitt-Gray PhD mmcnittgray@mednet.ucla.edu, Jonathan G. Goldin MbChB PhD jgoldin@mednet.ucla.edu, Matthew S. Brown PhD mbrown@mednet.ucla.edu, Hyun J. Kim MS gracekim@mednet.ucla.edu, Kathleen Brown MD kbrown@mednet.ucla.edu, Denise R. Aberle MD daberle@mednet.ucla.edu,

Corresponding Address: 924 Westwood Blvd. Suite 650, Box 957319, Los Angeles, CA 90095-7319, USA

Pulmonary Nodule Characterization: A Comparison of Conventional with Quantitative and Visual Semi-Quantitative Analyses Using Contrast Enhancement Maps

with an average AUC of 0.79. From the statistical analysis performed to combine the texture features to a single factor, the area under the ROC curve was 0.84.

Conclusion— The present study suggests that visual semi-quantitative and quantitative characterization of contrast enhancement patterns may potentially enhance the discrimination between benign and malignant nodules. Further studies and correlation with pathologic material will be important to better understand the potential interplay between CT enhancement features, host stromal elements, and neovascularity that may contribute to these patterns.

Keywords

CT; enhancement; lung cancer; pattern; texture; diagnosis

Introduction

Lung cancer is the most frequently occurring cancer in the world, and the leading cause of cancer death in both men and women in the United States (1). Non small cell lung cancer (NSCLC) accounts for approximately 75% of all lung cancers. On CT, lung cancer commonly manifests as a non-calcified pulmonary nodule. The increasing use of CT for pulmonary applications, including its potential use as a screening tool for early lung cancer detection, has magnified the need to develop better non-invasive methods for distinguishing benign from malignant nodules (2–9).

The prevalence of indeterminate lung nodules in published screening CT studies varies depending upon the size of nodule considered. In the Early Lung Cancer Action Project (ELCAP), non-calcified nodules were detected in 23% of participants by low-dose CT at baseline, compared with 7% by chest radiography (2). Diedrich and colleagues detected one or more nodules in 50% of screening CT scans in a high risk cohort (3). Swensen et al. found that 51% of low dose screening CT examinations revealed lung nodules (4). Only 1–10% of indeterminate nodules will eventually be diagnosed as malignant (2,3,6–9); the vast majority of cancers being larger than 4 mm diameter at first detection. While most nodules detected on screening are sub-centimeter in diameter, and the mean size of CT-detected cancers detected ranges from 13.4 mm to 18 mm (4, 6, 7 and 9), it is still important to develop reliable non-invasive methods for identifying malignant lesions.

Despite high spatial resolution, CT morphology alone is insufficient to distinguish reliably between benign and malignant nodules. With dynamic contrast enhanced-CT (DCE-CT), the absence of contrast enhancement has been shown to have high negative predictive value (10). Using post-contrast enhancement of 15 Hounsfield units (HU) as the minimum threshold for enhancement, one multicenter trial found DCE-CT sensitivity and specificity to be 98% and 58%, respectively (10). The lack of specificity relates to the fact that more than 50% of benign nodules enhance at least 15 HU (10). High false positive rates contribute to unnecessary invasive procedures, such as percutaneous or open biopsy, the latter being associated with an approximately 20% rate of futile thoracotomy (11).

In previous research, benign and malignant cases have been differentiated in a non-visual quantitative feature space. This work showed the potential of combining multiple features to provide better separation between groups than using individual features (12). Contrast enhancement features afford additional characterization as a surrogate of angiogenesis, which is a fundamental attribute of malignant neoplasms. Based on current literature, the extent of enhancement on DCE-CT is associated with the extent of nodular angiogenesis (13).

In this study, we were interested in investigating various methods to discriminate between benign and malignant lesions on the hypothesis that visual, semi-quantitative and quantitative

analyses of contrast enhancement maps may outperform conventional measures of mean attenuation from DCE-CT nodule densitometry.

Methods and Materials

Pulmonary nodule database

Beginning May 1998 through November 2002, CT data sets (volumetric thin-section scans covering the entire length of the nodule) were collected from 29 patients (15 men, 14 women; age range, 34–85 years; mean, 61 years), for the evaluation of an indeterminate solitary pulmonary nodule. All participants in whom the same standardized DCE-CT protocol was performed were included if pathological diagnosis of the nodule was available or long term follow up satisfied clinically accepted definitions of benignity. While the authors cannot guarantee that the patients were consecutive, no patients who met these clinical and imaging criteria were excluded. The diagnosis of each nodule was determined through pathology reports or radiological follow-up of at least two years. There were 15 malignant nodules with pathologic confirmation (9 men, 6 women; age range, 51–85 years; mean, 70 years): 13 primary lung carcinomas (six adenocarcinomas, two bronchioloalveolar cell carcinomas, one squamous cell carcinoma, one undifferentiated non-small cell carcinoma, one neuroendocrine tumor, one large cell adenocarcinoma with neuroendocrine differentiation, and one adenosquamous carcinoma) and two metastatic lesions (adenocarcinoma of colonic and prostate primary origins) (Table 1). Benign nodules were diagnosed in 14 patients (6 men, 8 women; age range, 34–81 years; mean, 53 years): four granulomas, two necrotizing granulomas, one sclerosing hemangioma, one benign mesenchymal tumor, and five clinically benign lesions stable for more than two years of radiological follow-up (Table 1). All nodules were non-calcified, non-cavitary lesions and ranged from 6 to 58 mm (mean diameter, 24 mm; median diameter, 22 mm; standard deviation, 12 mm). Benign nodules ranged from 10 to 32 mm (mean diameter, 19 mm; median diameter, 19 mm; standard deviation, 7 mm) and malignant nodules ranged from 6 to 58 mm (mean diameter, 28 mm; median diameter, 28 mm; standard deviation, 14 mm). Three lesions were over 30 mm diameter, but were included in the study because they were indeterminate at the time of scanning and had been referred for DCE-CT. The study was conducted and all data was collected with the approval of the local institutional review board. Written consent was obtained in 12 patients; in 17 patients, approval was obtained for retrospective data collection.

CT protocol

Dynamic contrast enhanced chest CT (DCE-CT) was performed on all patients. Scans were performed on the following two-detector CT platforms: the GE HiSpeed CT/I (n=14), GE HiSpeed Advantage (n=13), (GE Medical Systems, Milwaukee, WI) or the Picker PQ 5000 (n=2), (Picker International, now Philips Medical Systems, Cleveland, OH). Technical parameters were: 120 kVp, 200–280 mAs, $\leq$3 mm slice thickness and either contiguous (16/29) or overlapped (13/29) reconstruction interval, with the reconstruction diameter spanning the bony chest wall. A standard reconstruction filter without high spatial frequency enhancement was used. The baseline series was a non-contrast, helical sequence that covered the entire nodule. Following this, dynamic contrast-enhanced nodule densitometry was performed, consisting of four volumetric sequences through the nodule post-bolus administration of IV contrast (100 cc; 2 cc/sec; [Omnipaque 350; Amersham Biosciences, now part of GE Healthcare, Piscataway, NJ]). The post-contrast sequences were timed in similar fashion to the protocol previously published at 45, 90, 180, and 360 seconds post-initiation of the contrast injection, using identical acquisition parameters and slice thicknesses as the baseline, pre-contrast series (10).

Generating the contrast enhancement maps

The three-dimensional (3D) boundaries of all nodules on each series (pre- and post-contrast) were obtained by semi-automated contouring with manual editing as needed. A 3D ROI was generated by selecting a seed point within the nodule, from which a region growing algorithm was performed using adjustable attenuation thresholds to segment the nodule. The mean attenuation of the 3D ROI was calculated on the baseline and each of the four post-contrast series. The post-contrast series with the maximum mean attenuation (relative to baseline) was then volumetrically registered to the baseline series using a 3D affine transformation that was optimally selected when using a mutual information metric (14). Corresponding axial images from the baseline and the registered post-contrast series were subtracted to create a volume of difference image data; the difference voxels were quantized into seven color-coded bins (Figure 1b), creating the CEM. A single slice of the CEM is illustrated in Figure 1a.

Analyses of the contrast enhancement maps

Conventional Nodule Densitometry—Mean peak enhancement was calculated as the difference in mean values from a circular ROI between post-contrast and baseline series, as described by Swensen (10). Note that this circular ROI is *not* the same ROI created by the radiologist to determine the nodule boundary. The enhancement value was measured for each nodule. Using this approach, enhancement values≤U are indicative of benign nodules.

Visual Semi-quantitative Analyses—Three thoracic radiologists (10+ years experience; blinded to nodule diagnosis), visually scored each individual contrast enhancement map in 3D for: magnitude of enhancement and the overall pattern or heterogeneity of enhancement. The magnitude of enhancement was defined as the degree of peak enhancement within the nodule. Magnitude was visually scored on a 5-point scale (1-none, 2-minimal, 3-mild, 4-moderate, 5-extensive [Figures 2, 3]). Pattern of enhancement (visually scored on a 5-point scale: 1-homogenous, 2-moderately homogeneous, 3-intermediate, 4-moderately heterogeneous, 5-heterogenous [Figures 2, 3]) was designed to measure the relative heterogeneity of the pattern of enhancement (attenuation) throughout the entire volume of the nodule. Thoracic radiologists were trained by the research associate on a computer-simulated CEM with varying magnitudes and patterns of enhancement. Radiologists were asked to score explicitly the visual magnitude and pattern of enhancement, without consideration of other nodule features, such as size or border characteristics.

During the scoring of test nodules, radiologists were also provided the matched pre-contrast and maximum post-contrast images used to create the difference maps at all axial levels. This was done to provide the reading radiologist with additional perspective in determining the quality of the registration process and the subsequent validity of the appearance of attenuation patterns. In addition, a histogram of the color-coded voxels was created. The histogram was formed from the entire 3D nodule volume, whereby the number of voxels in each bin was quantified and plotted on a bar graph. Each bar was color-coded to the same color as the voxels that it represented. The histogram was intended to provide an additional quantitative representation of the enhancement characteristics of the nodule (Figure 1b).

Quantitative Analyses—Fourteen co-occurrence, matrix-based textural features representing mathematical descriptors of the spatial variation of the subtracted voxels were calculated (15). Each co-occurrence matrix was formed at a distance of one-voxel between neighboring voxels. Due to the small number of cases compared to the number of features, dimension reduction techniques were invoked to evaluate the ability of these features to characterize different nodules. The 14 individual features were grouped into six related sets of features. These sets included features that captured the range and average of entropy, correlation, and variance of the texture. Principal components analyses (PCA) was performed

separately on each of these six groups, and the principal component containing the highest proportion of variance was chosen. This resulted in six components that were then introduced into the factor analysis. The dimension was reduced to one factor by first performing PCA on six groups of variables. The component that encapsulated the greatest amount of variance was extracted for each of the six groups. Factor analysis was then performed on these six components to derive one final aggregate factor.

Statistical Analyses

As part of the conventional analysis, and using the protocol described by Swensen (10), 15 HU was used as the threshold to distinguish benign from malignant nodules. The sensitivity, specificity, positive predictive value, and negative predictive value were calculated for our dataset of nodules. Additionally, the same calculations were performed at thresholds of 20 HU, 30 HU and 50 HU.

All features in our study were analyzed for differences between benign and malignant nodules. ROC analysis was conducted on the peak enhancement, qualitative magnitude and pattern of enhancement, and the derived quantitative feature, on the assumption that higher values for each of these elements reflect malignancy. ROC curves were fitted and the area under the curve (AUC) was calculated using PROPROC (Version 1.0 beta, University of Chicago; Chicago, IL).

Results

Conventional Evaluation

Using 15 HU as the threshold to distinguish malignant from benign nodules, 93% (14/15) of malignant nodules and 79% (11/14) of benign nodules demonstrated enhancement, resulting in 93% sensitivity, 21% specificity, a positive predictive value of 56%, and a negative predictive value of 75% (Table 2). The results for thresholds of 20 HU, 30 HU and 50 HU are also summarized in Table 2. Overall, increasing the threshold attenuation compromised the sensitivity of the test while providing only marginal improvements in specificity. The ROC curve, when higher values of the enhancement indicate malignancy, had an AUC of 0.76 (Figure 4).

Visual semi-quantitative Evaluation

ROC analysis was conducted independently for both magnitude and pattern of enhancement (Figure 5 and 6). The magnitude of enhancement was less effective in distinguishing benign from malignant lesions, with an average AUC of 0.62 (Figure 5). Greater discrimination was achieved with pattern of enhancement, with an average AUC of 0.79 (Figure 6). Overall, radiologists observed more homogenous patterns of enhancement in benign nodules (Figure 2) and more heterogeneous enhancement in malignant nodules (Figure 3).

Quantitative Evaluation

The proportion of variance from the factor analysis incorporated 94% of the total variation. ROC analysis of the derived single aggregate factor as an indicator of malignancy was performed. When using this final aggregate factor, the AUC was 0.84 (Figure 7).

Discussion

Diagnostic pathways to distinguish benign and malignant nodules vary, but generally involve one or more of the following: (a) repeat CT examinations over time to detect growth, (b) DCE-CT to assess nodule enhancement, (c) positron emission tomography (PET) with 2-[fluorine-18] fluoro-2-deoxy-D-glucose (FDG) to detect increased glucose metabolism as an

index of malignancy, or (d) percutaneous, bronchoscopic or open biopsy. Repeat CT examinations are commonly performed for small sub centimeter nodules too small to characterize by other methods, but carry some risk from cumulative radiation exposure and can be psychologically costly. Both DCE-CT and PET have been validated in clinical trials, however have well-known limitations. Dynamic contrast-enhanced CT is only effective for its negative predictive value and in lesions of at least 7 to 8 mm in diameter. FDG PET is inconsistent with certain malignant histologies such as bronchioloalveolar cell carcinoma and carcinoid lesions, as well as for nodules in the peri-centimeter size range now routinely detected with CT. Finally, biopsy procedures carry certain risks and may also be indeterminate due to sampling error, particularly with small lesions. To investigate approaches differing from conventional CT nodule densitometry, we analyzed 3D contrast enhancement maps (visual scoring of their magnitude of enhancement, visual scoring of their pattern of enhancement and quantitative texture analyses) and have presented our results using ROC analyses. We listed AUC values for the various analytic methods, but cannot compare differences between ROC curves as we have insufficient nodules in our dataset to make significant comparisons. However, we postulate that these features/approaches may provide complementary information. It will be possible to make these comparisons in future research with a larger dataset, as well as to combine features (i.e. quantitative texture and subjective markings) to determine if they are complementary.

The basis for DCE-CT in nodule characterization is that the microvascular changes of tumor angiogenesis are reflected by increased tumor perfusion *in vivo*. Tumor-induced angiogenesis is the process by which new blood vessels are formed from existing vessels, a process essential for both tumor growth and metastasis (16). It has been suggested that the increased perfusion of angiogenesis results in increased contrast enhancement (measured by peak and net enhancement) to a magnitude determined by the intensity of angiogenesis (13,17).

Angiogenic blood vessels are highly permeable (17,18), and allow macromolecules such as iodine and plasma proteins to enter stroma (19). Blood vessel leakiness contributes to high interstitial pressures, and in regions of high vascular permeability compresses the microcirculation (19–23), resulting in tissue hypoxia and necrosis.

Although the microcirculation itself cannot be visualized with CT, the resulting regional variations in tissue microvessel density, local blood flow, and tumor necrosis contribute to heterogeneous enhancement patterns within a given tumor, and may provide both visual and quantifiable measures of tumor angiogenesis that transcend global measures of mean attenuation from a tumor ROI. We postulate that the heterogeneity seen with malignant neoplasms in our data set is a reflection of the complex vascular environment of malignant tumors.

There were several limitations in our study. First, our data set was relatively small, limiting our ability to validate the significance of patterns of enhancement and quantitative feature analysis on contrast enhancement maps. In addition, as only nodules with histologic confirmation or long term follow-up were selected, unintentional selection bias could have been introduced. Moreover, our data set included both primary and metastatic lesions of lung, which may exhibit different patterns of vascularity that would affect enhancement on DCE-CT. Our results of conventional evaluation showed lower sensitivity, specificity and positive/negative predictive values in comparison with the literature, which suggests that our small sample size may not be representative of the general population. Of note, the quantitative analyses of the CEM were not tailored to this particular set of 29 subjects. However, given the small dataset, the results may be optimistic due to potential overfitting from aggregating 14 features and because the small numbers of nodules precluded creation of separate training and testing datasets.

Second, we observed moderate inter-reader variability (a known limitation of visual scoring methods [24]), though no clear explanation for this can be cited; all three radiologists are equally experienced, and were trained on a computer-simulated CEM in an attempt to visually calibrate the readers.

Third, is the potential error introduced from misregistration (during the pixel by pixel subtraction of the baseline from peak enhancement series) due to breathing and cardiac motion between the series. We cannot guarantee the fidelity of our registration process; however, all nodules were visually inspected in three dimensions to ensure faithful registration of the nodule margins from the different series.

Fourth, timing of enhancement is also a potential limitation when evaluating angiogenesis. We followed a published protocol for DCE-CT in which five series are acquired through the nodule at baseline and at four time points post-initiation of a contrast bolus. Although there is historical precedence for using this protocol, the limited temporal sampling frequency constrains the richness of the time-attenuation characteristics of the nodules. Malignant nodules generally exhibit shorter time of peak enhancement and a higher slope of enhancement, due in part to the higher microvessel density (MVD) (13). A higher sampling frequency early in the contrast injection is needed to capture this enhancement behavior (25). Similarly, the washout phase of malignant nodules provides valuable information due to the persistence of iodine that extravasates into the interstitial spaces from leaky vessels, and requires that late imaging be performed. Recent work has illustrated the value of combined wash-in and washout characteristics of solitary pulmonary nodules at dynamic CT, with 92% accuracy in distinguishing benign from malignant nodules (26). Of note, these authors used extended imaging protocol (scanning as late as 15 minutes after injection) to estimate the wash-out (26). We acquired images at five minutes post-injection, but the characteristics of the time-attenuation curve are uncertain with so few time points measured.

In patients with primary and metastatic solid tumors, size measurements derived from CT historically have been the mainstay in determining response assessment to cytotoxic therapies. With new cytostatic agents and drugs that affect angiogenesis, decreases in tumor volume may not occur if drug-induced metabolic alterations precede tumor shrinkage, or if scar and necrosis replace viable tumor without changes in overall size. Therefore, size alone may not accurately predict treatment efficacy (27). We consider the CT contrast enhancement maps to be a potentially important method to follow treatment response, particularly in patients receiving anti-angiogenic therapy.

Using imaging to approach tumor heterogeneity, from an angiogenesis perspective, is challenging to scientists. Microscopic methods provide their highest resolution on preserved tissue specimens, whereas clinical methods can image living tissue deep within a tumor, but at a resolution too low to see the microcirculation (18). The continuing question is how to account for tumor heterogeneity in the most truthful way. There is little consensus on the best standards of validation of the many methods for imaging angiogenesis (18). Clinical studies have suggested that tumor angiogenesis, as characterized by MVD count, correlates well with poor prognosis and tumor metastasis (28,29). It will be interesting to correlate the contrast enhancement map with the MVD of nodules, as MVD is considered the standard for quantification of angiogenesis in histological studies. Chin A Yi et al. (13) have published a comparison of dynamic CT study with vascular endothelial growth factor (VEGF) and MVD, reporting significant positive correlations between the extent of peak enhancement and tumor angiogenesis, irrespective of the malignant or benign nature of the nodule. In their dataset, VEGF expression was significantly higher in malignant vs. benign nodules. VEGF is one of the many endogenous promoters of angiogenesis and a multifunctional cytokine that contributes to angiogenesis by both direct and indirect mechanisms (19). VEGF

immunostaining can be used as a potential starting point for validation of different enhancement patterns observed in our study.

We are currently in the process of [1] correlating these color maps with MVD and immunohistochemical staining of VEGF in available tissue specimens to determine their relationships, [2] combining the CT data with that of FDG-PET uptake and [3] correlating them with clinical outcomes to determine whether they can provide insights into the biological behavior of neoplasms.

Tumor angiogenesis has significant implications in the diagnosis and treatment of pulmonary nodules, and as such, developing techniques to characterize and quantify tumor angiogenesis would be important in the management of lung tumors.

Conclusion

The present study suggests that visual semi-quantitative and quantitative characterization of contrast enhancement patterns, derived from 3D-contrast enhancement maps, may potentially enhance the discrimination between benign and malignant nodules. CEM provide a visual representation of the regional variations in enhancement resulting from the complex microcirculation and physiology of angiogenic vessels. Further studies and correlation with pathologic material will be important to better understand the potential interplay between CT enhancement features, host stromal elements, and neovascularity that may contribute to these patterns.

Acknowledgements

Funded by NCI grants: UCLA SPORE in lung cancer 5P50CA090388-04 and R01-CA83903 We would like to thank Brandon Brett Bigby, B.A. for providing help with editing this manuscript.

References

1. Alberg AJ, Samet JM. Epidemiology of lung cancer. Chest 2003;123(Suppl):21S–49S. [PubMed: 12527563]
2. Henschke CI, McCauley DI, Yankelevitz DF, et al. Early Lung Cancer Action Project: overall design and findings from baseline screening. Lancet 1999;354(9173):99–105. [PubMed: 10408484]
3. Diederich S, Wormanns D, Semik M, et al. Screening for early lung cancer with low-dose spiral CT: prevalence in 817 asymptomatic smokers. Radiology 2002;222(3):773–81. [PubMed: 11867800]
4. Swensen SJ, Jett JR, Hartman TE, et al. CT screening for lung cancer: five-year prospective experience. Radiology 2005 Apr;235(1):259–65. [PubMed: 15695622]Epub 2005 Feb 4.
5. Hillman BJ. Economic, legal, and ethical rationales for the ACRIN national lung screening trial of CT screening for lung cancer. Acad Radiol 2003;10(3):349–50. [PubMed: 12643562]
6. Pastorino U, Bellomi M, Landoni C, et al. Early lung-cancer detection with spiral CT and positron emission tomography in heavy smokers: 2-year results. Lancet 2003;362(9384):593–7. [PubMed: 12944057]
7. Swensen SJ, Jett JR, Hartman TE, et al. Lung cancer screening with CT: Mayo Clinic experience. Radiology 2003;226(3):756–61. [PubMed: 12601181]
8. Swensen SJ, Jett JR, Sloan JA, et al. Screening for lung cancer with low-dose spiral computed tomography. Am J Respir Crit Care Med 2002;165(4):508–13. [PubMed: 11850344]
9. Sone S, Li F, Yang ZG, Honda T, et al. Results of three-year mass screening programme for lung cancer using mobile low-dose spiral computed tomography scanner. Br J Cancer 2001;84(1):25–32. [PubMed: 11139308]
10. Swensen SJ, Viggiano RW, Midthun DE, et al. Lung nodule enhancement at CT: multicenter study. Radiology 2000;214(1):73–80. [PubMed: 10644104]

11. Crestanello JA, Allen MS, Jett JR, Cassivi SD, Nichols FC III, et al. Thoracic surgical operations in patients enrolled in a computed tomograpic screening trial. J Thorac Cardiovas Surg 2004;128:254–259.
12. Shah SK, McNitt-Gray MF, Rogers SR, et al. Computer Aided Characterization of the Solitary Pulmonary Nodule Using Volumetric and Contrast Enhancement Features. Acad Radiol 2005 Oct; 12(10):1310–9. [PubMed: 16179208]
13. Yi CA, Lee KS, Kim EA, et al. Solitary Pulmonary Nodules: Dynamic Enhanced Multi–Detector Row CT Study and Comparison with Vascular Endothelial Growth Factor and Microvessel Density. Radiology 2004;233:191–199. [PubMed: 15304661]
14. Mattes D, Haynor D, Vesselle H, Lewellen T, Eubank W. Nonrigid multimodality image registration. SPIE Int. Soc. Opt. Eng Proceedings of Spie the International Society for Optical Engineering, vol 2001;4322:1–3.
15. Haralick R, Shanmugam K, Dinstein I. Textural features for image classification. IEEE Transactions on Systems, Man & Cybernetics 1973;(6):610–21.
16. Folkman J. Tumor angiogenesis: therapeutic implications. N Engl J Med 1971 Nov 18;285(21):1182–6. [PubMed: 4938153]
17. Miles KA. Tumour angiogenesis and its relation to contrast enhancement on computed tomography: a review. Eur J Radiol 1999 Jun;30(3):198–205. [PubMed: 10452718]
18. McDonald DM, Choyke PL. Imaging of angiogenesis: from microscope to clinic. Nat Med 2003 Jun; 9(6):713–25. [PubMed: 12778170]
19. Dvorak HF, Brown LF, Detmar M, Dvorak AM. Vascular permeability factor/vascular endothelial growth factor, microvascular permeability, and angiogenesis. Am J Pathol 1995;146:1029–39. [PubMed: 7538264]
20. Vaupel P, Kallinowski F, Okunieff P. Blood flow, oxygen and nutrient supply, and metabolic microenvironment of human tumors: a review. Cancer Res 1989;49:6449–65. [PubMed: 2684393]
21. Baillie CT, Winslet MC, Bradley NJ. Tumor vasculature: a potential therapeutic target. Br J Cancer 1995;72:257–67. [PubMed: 7543770]
22. Jain RK. Determinants of tumor blood flow: a review. Cancer Res 1988;48:2641–58. [PubMed: 3282647]
23. Tumor Angiogenesis. Oxford University Press; Oxford: 1997. Vascular and Interstitial Physiology of Tumours: Role in Cancer Detection and Treatment; p. 45
24. Malinen A, Erkinjuntti-Pekkanen R, Partanen K, Rytkönen H, Vanninen R. Reproducibility of scoring emphysema by HRCT. Acta Radiol 2002 Jan;43(1):54–9. [PubMed: 11972463]
25. Miles KA. Perfusion CT for the assessment of tumour vascularity: which protocol? Br J Radiol 2003;76:Spec No 1:S36–42.
26. Jeong YJ, Lee KS, Jeong SY, et al. Solitary Pulmonary Nodule: Characterization with Combined Wash-in and Washout Features at Dynamic Multi–Detector Row CT. Radiology 2005 Nov;237(2): 675–83. [PubMed: 16244276]
27. Li WW. Tumor angiogenesis: molecular pathology, therapeutic targeting, and imaging. Acad Radiol 2000 Oct;7(10):800–11. [PubMed: 11048878]
28. Weidner N. Intratumor microvessel density as a prognostic factor in cancer. Am J Pathol 1995;147:9–19. [PubMed: 7541613]
29. Prognostic and predictive value of intra-tumoral microvessel density in human solid tumours. In: Bicknell, R.; Lewis, CE.; Ferrara, N., editors. Tumour angiogenesis. Oxford: Oxford University Press; 1997. p. 29-44.

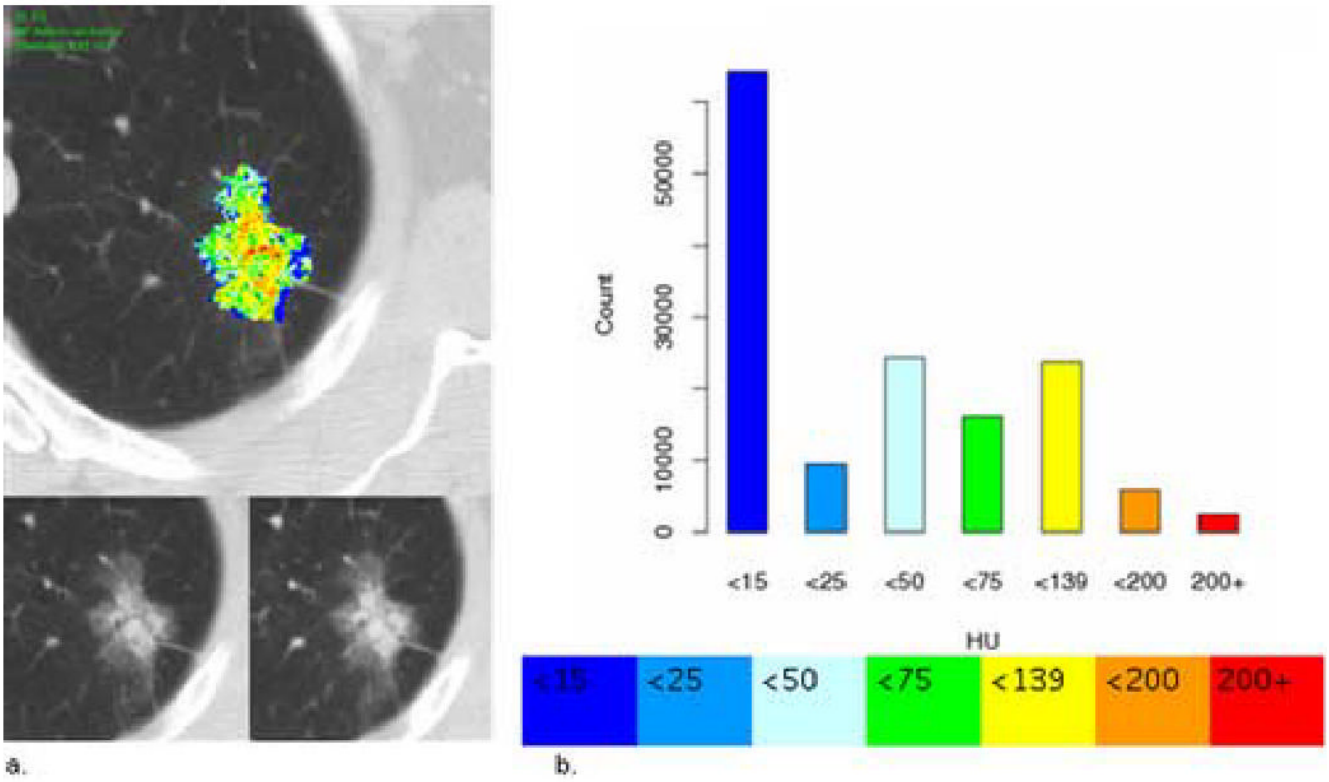

Figure 1.
Contrast enhancement map. (a) Top: Contrast enhancement map (CEM) of an adenocarcinoma through the axial equator (single, two-dimensional [2D] representative slice from the complete 3D ROI). This nodule was visually graded by the three readers as moderate magnitude of enhancement (mean magnitude score 4) and moderate to high heterogeneity (mean pattern score 4.3). Bottom: Matched pre-contrast (left) and maximum post-contrast images (right) used to create the difference image, respectively. (b) Top: Histogram showing the color-coded voxel frequency distribution from the corresponding complete 3D ROI of the nodule. Bottom: Colors used to quantize the attenuation differences (HU).

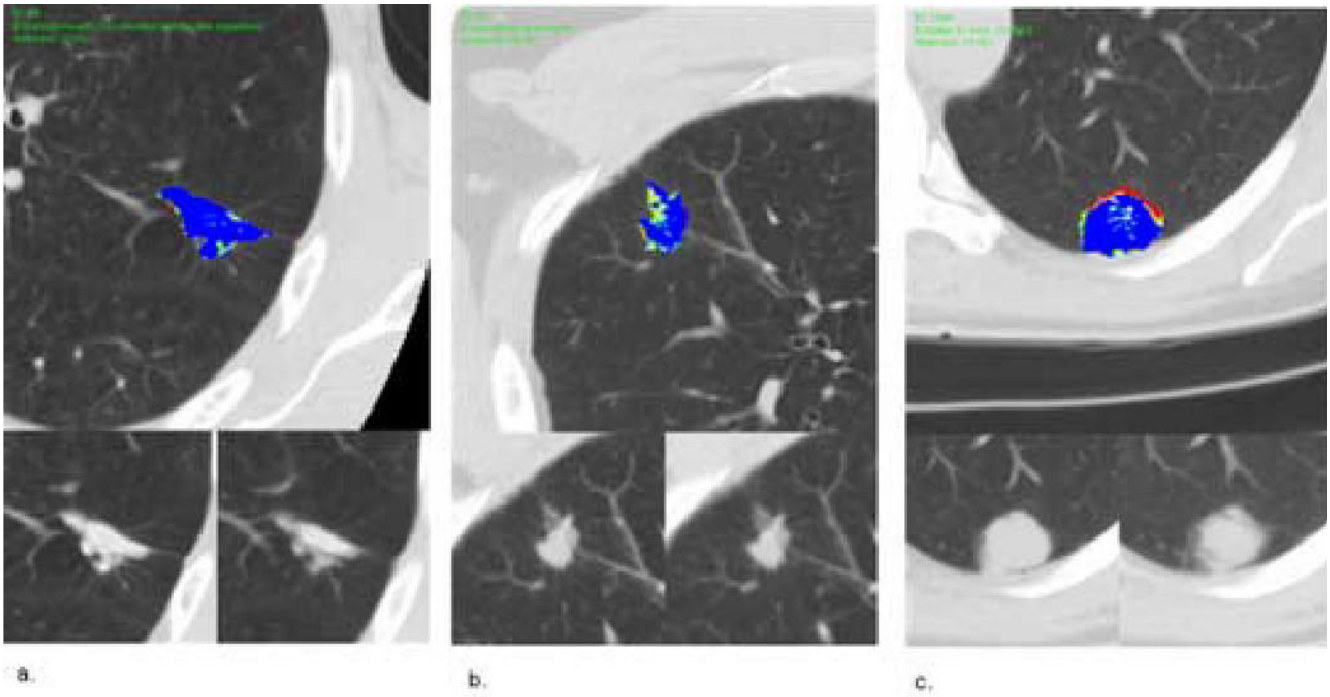

Figure 2.

Benign nodules. (a) Top Image: Contrast enhancement map (CEM) of a benign nodule through the axial equator, granuloma with Coccidioides immitis-like organisms. Lower left: pre-contrast image. Lower right: maximum enhancement post-contrast image. Mean magnitude score 3, mean pattern score 2.7. (b) Top Image: contrast enhancement map of a benign nodule through the axial equator, necrotizing granuloma. Lower left: pre-contrast image. Lower right: maximum enhancement post-contrast image. Mean magnitude score 1.7, mean pattern score 1.7. (c) Top Image: contrast enhancement map of a benign nodule through the axial equator, stable > 2 years on radiological follow-up. Lower left: pre-contrast image. Lower right: maximum enhancement post-contrast image. Mean magnitude score 3.3, mean pattern score 2.7.

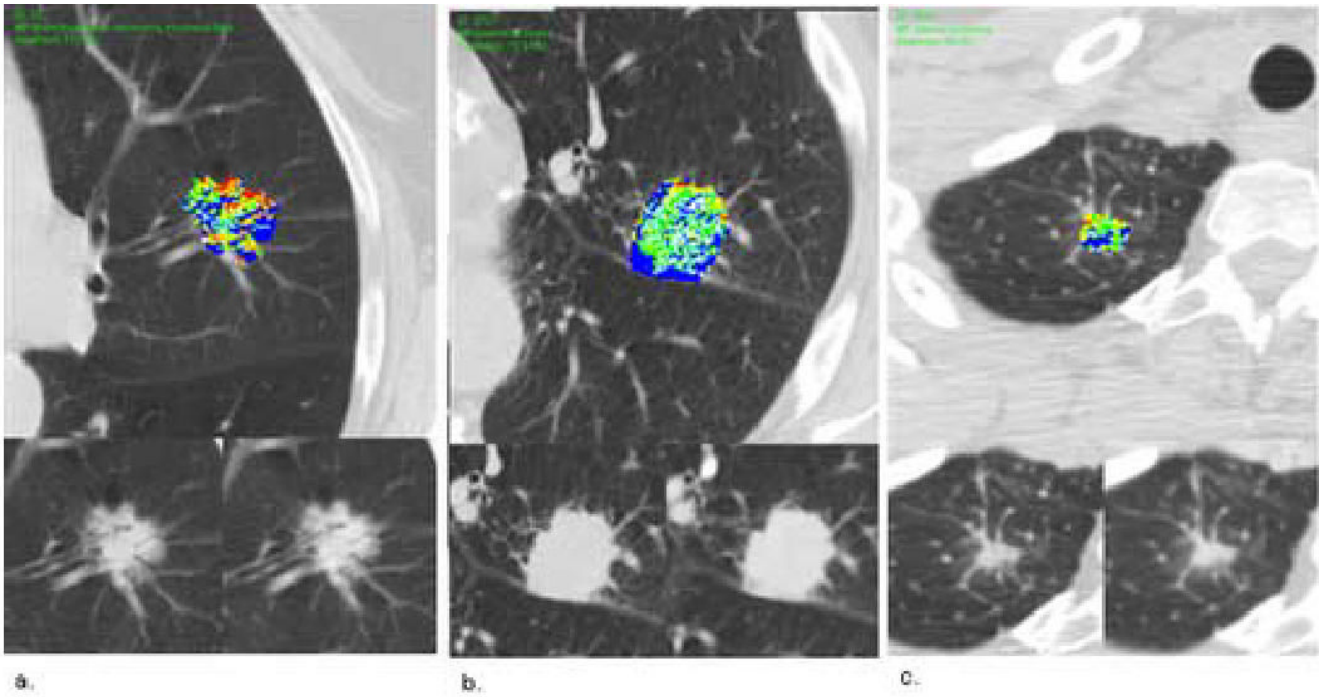

Figure 3.
Malignant nodules. (a) Top Image: contrast enhancement map of a malignant nodule through the axial equator, bronchioalveolar carcinoma, mucinous type. Lower left: pre-contrast image. Lower right: maximum enhancement post-contrast image. Mean magnitude score 3.7, mean pattern score 4. (b) Top Image: contrast enhancement map of a malignant nodule through the axial equator, adenocarcinoma. Lower left: pre-contrast image. Lower right: maximum enhancement post-contrast image. Mean magnitude score 3.3, mean pattern score 4.3. (c) Top Image: contrast enhancement map of a malignant nodule through the axial equator, adenocarcinoma. Lower left: pre-contrast image. Lower right: maximum enhancement post-contrast image. Mean magnitude score 4, mean pattern score 4.3.

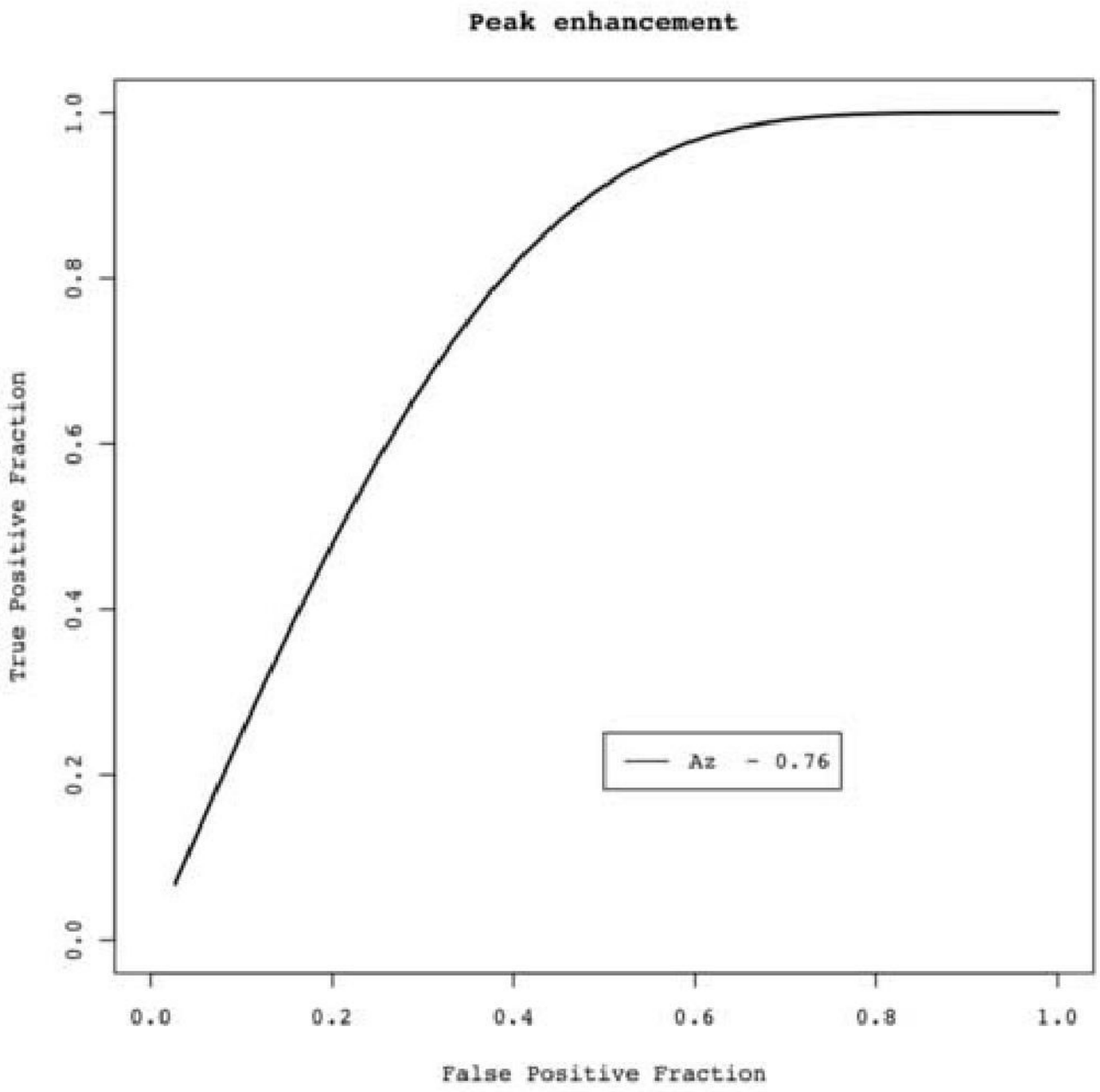

Figure 4.
ROC curve using conventional peak enhancement analysis. Area under the curve (Az) = 0.76.

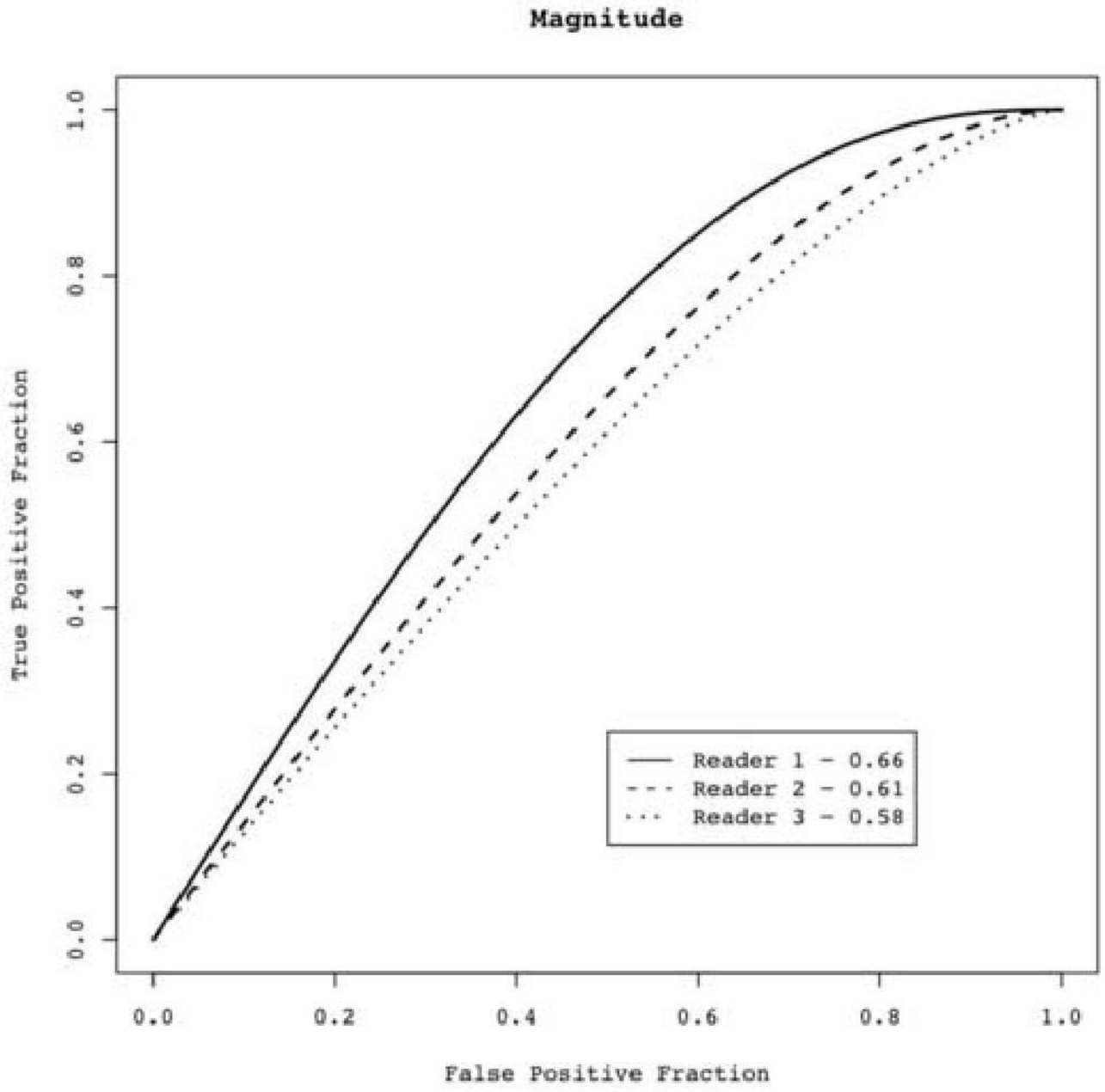

Figure 5.
ROC curve showing results from three readers' subjective visual semi-quantitative assessment of magnitude of enhancement. Readers used a 5-point scale: 1-none, 2-minimal, 3-mild, 4-moderate, 5-extensive. Area under the curve (Az) ranged from 0.58 to 0.66, with an average of 0.62.

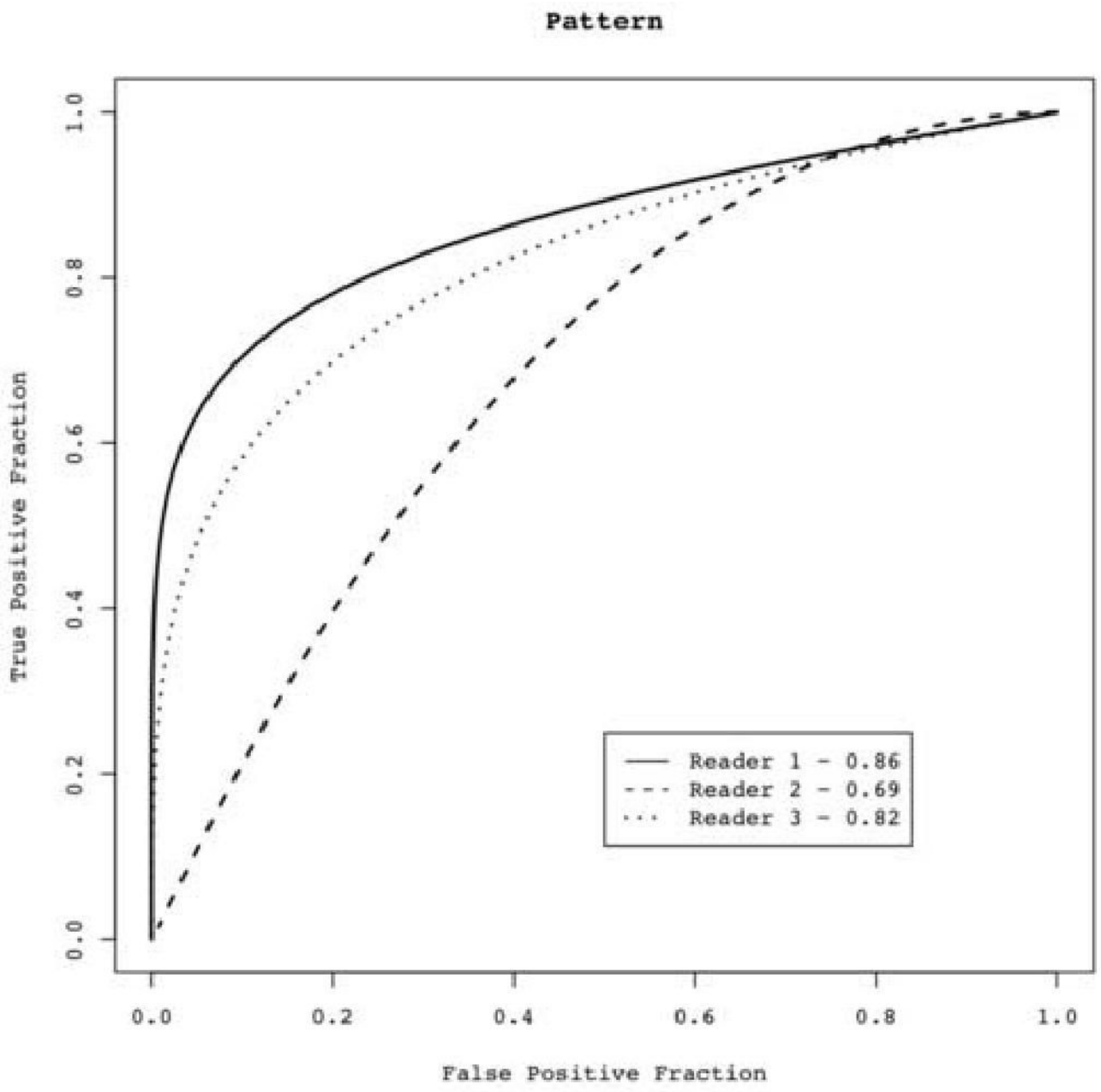

Figure 6.
ROC curve showing results from three readers' subjective visual semi-quantitative assessment of pattern of enhancement. Readers used a 5-point scale: 1-homogenous, 2-moderately homogeneous, 3-intermediate, 4-moderately heterogeneous, 5-heterogenous. Area under the curve (Az) ranged from 0.69 to 0.86, with an average of 0.79.

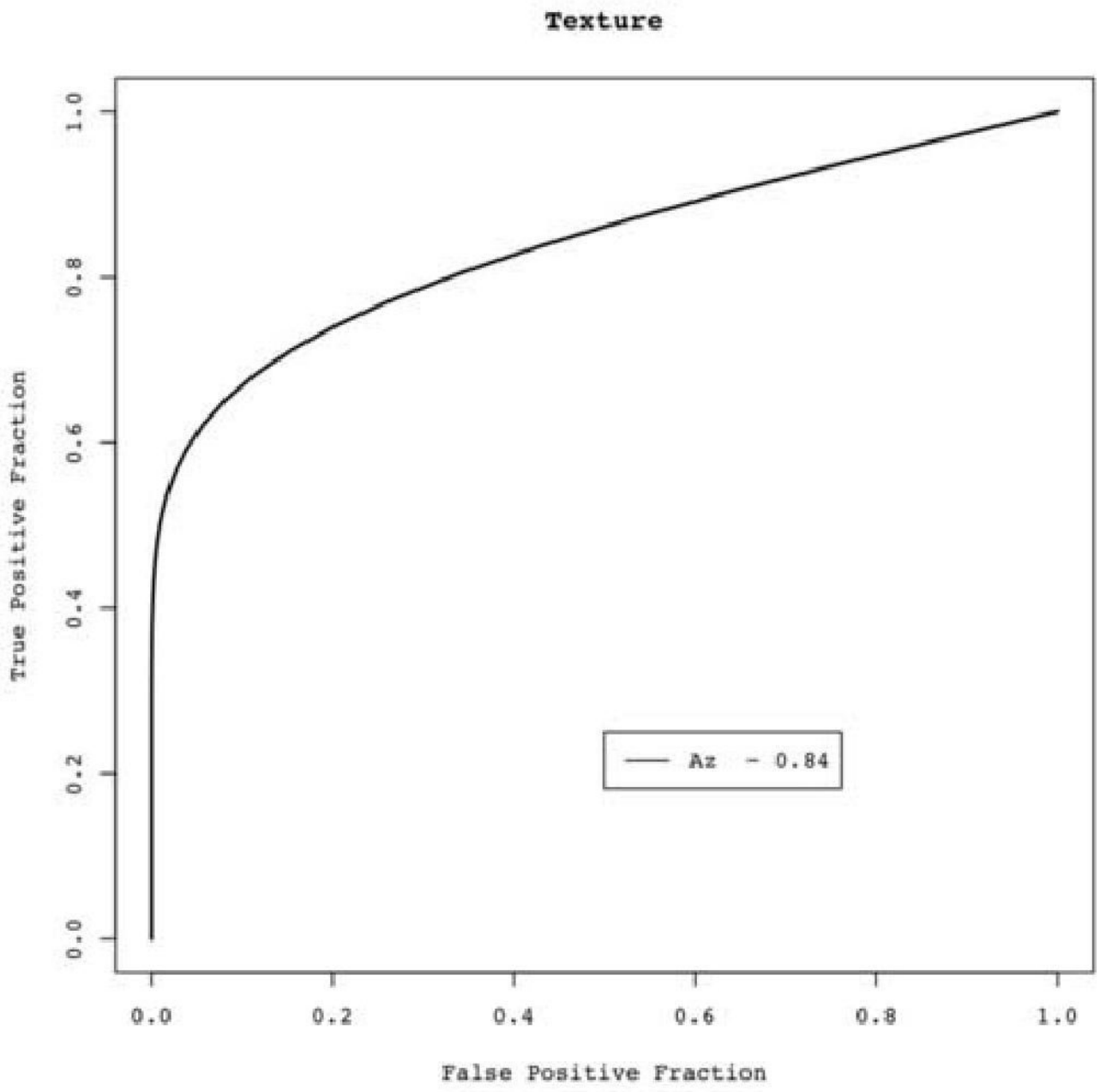

Figure 7.
ROC curve using a single aggregate texture measure derived direct from image data (quantitative objective measure). Area under the ROC curve (Az) = 0.84.

Table 1

Clinical and Pathologic Diagnoses of the Nodules

Nodule diagnosis	Nodule type	No
Malignant primary (n=13)	Adenocarcinoma	6
	Bronchioalveolar carcinoma	2
	Undifferentiated non-small cell carcinoma*	1
	Squamous cell carcinoma	1
	Neuroendocrine tumor	1
	Large cell adenocarcinoma with neuroendocrine differentiation	1
	Adenosquamous carcinoma	1
Malignant metastatic (n=2)	Adenocarcinoma of colonic origin	1
	Adenocarcinoma of prostate origin	1
Benign (n=14)	Granuloma	4
	Necrotizing Granuloma	2
	Sclerosing hemangioma	1
	Benign mesenchimal tumor**	1
	Histology negative***	1
	Radiologically stable (>24 months)	5

* This nodule was determined at pathology to be malignant; however no further histologic characterization was established.

** This nodule was determined at pathology to be benign mesenchymal tumor; however no further histologic characterization was established.

*** This nodule was determined at pathology to be benign; however no further histologic characterization was established.

Table 2

Sensitivity and Specificity of Mean Peak Enhancement at Different Attenuation Thresholds

Attenuation Threshold	Sensitivity	Specificity	PPV	NPV
15HU	93%	21%	56%	75%
20HU	93%	36%	61%	83%
30HU	60%	71%	69%	63%
50HU	47%	79%	70%	58%